Nuclear Science & Technology Research Institute

Journal of Nuclear Research and Applications

Research Paper

Journal homepage: https://jonra.nstri.ir

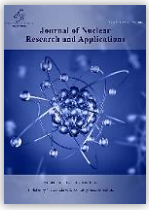

Development of Transient Dynamics Code for a Helically-Coiled Steam Generator Analysis Using Multi-Node Moving Boundary Model

A. Fakhraei*, F. Faghihi

School of Mechanical Eng., Shiraz University, P.O.Box: 71936-16548, Shiraz, Iran.

(Received: 2 August 2024, Revised: 15 November 2024, Accepted: 3 December 2024)

A B S T R A C T

Due to its compact design, higher heat transfer efficiency, and ability to produce superheated steam , helical coil steam generators (HCSG) have become a popular option for use in small modular reactors. This research focuses on developing a multi-node moving boundary model for the transient calculation of these steam generators. The secondary side of an HCSG consists of subcooled, two-phase, and superheated regions. The developed model can accurately track the boundaries of these phases and allocate their proportional heat transfer coefficients accordingly. Additionally, each region is divided into multiple nodes for more increased accuracy. This approach eliminates the need for fine nodes and phase detection in each node during each time step, significantly reducing the computational cost of calculating of steam generator behavior. Python programming language was used for computationsin this study, which greatly improved the speed and efficiency of the calculations. Furthermore, a RELAP5 model for HCSG was developed in this research . The results obtained from the developed code were compared against with RELAP5 calculated parameters. Multiple scenarios involving changes feedwater in properties and primary flow to the steam generator were modeled. The simulated scenarios demonstrate that both codes show similar trends for variations in the parameters. The methodology presented in this study can be applied to model HCSG dynamics in future studies.

Keywords: Small modular reactors; Helical coil steam generator; Multi-node moving boundary model; Steam generator dynamical simulation.

List of acronyms

DCA: Design Certification Application
HCSG: Helical Coil Steam Generator
HTGR: High Temperature Gas Reactor
IPWR: Integral Pressurized Water Reactor
LMFBR: Liquid Metal Fast Breeder Reactor
LOCA: Loss of Coolant Accident

*Corresponding Author E-mail: a.fakhraei@shirazu.ac.ir
DOI: https://doi.org/10.24200/jonra.2024.1626.1134.

LSODE: Livermore Solver for Ordinary Differential Equations

ODE: Ordinary Differential Equation

OTSG: Once Through Steam Generator

PWR: Pressurized Water Reactor

RELAP: Reactor Excursion and Leak Analysis Program

RPV: Reactor Pressure Vessel

SG: Steam Generator

SMR: Small Modular Reactor

Nomenclature

A: Flow area (m^2)

C_p: Specific heat capacity ($J.kg^{-1}.K^{-1}$)

C_w: Tube metal-specific heat ($J.kg^{-1}.K^{-1}$)

D: Diameter (m)

G: Mass flux ($kg.m^{-2}.s^{-1}$)

h: Enthalpy ($J.kg^{-1}$)

L: Height (m)

l: Subcooled liquid length (m)

$\dot{m}$: Mass flow rate ($kg.s^{-1}$)

n: Number of tubes

P: pressure(Pa)

T: Temperature(K)

t: Time (s)

x: x coordinate (m)

x_{ad}: Dry-out quality

Z: Vertical direction (m)

Special symbols

α_i: Inner tube heat transfer coefficient ($W.m^{-2}.K^{-1}$)

α_o: Outer tube heat transfer coefficient ($W.m^{-2}.K^{-1}$)

α: Void fraction

μ: Viscosity (Pa. s)

ρ: Density ($kg.m^{-3}$)

σ: Surface tension ($J.m^{-2}$)

Subscripts-superscripts

C: Coolant

S: Subcooled region

SG: Steam generator

T: Two-phase region

f: Liquid

fg: Two-phase property

g: Vapor

i: Inner surface

i: i_{th} volume

j: j_{th} boundary

o: Outer surface

pr: Primary

s: Secondary

tt: Two-phase property

w: Tube wall

1. Introductions

The steam generator is a crucial components of a nuclear reactor that connects the primary system to the secondary system. The design of the steam generator plays a pivotal role in reactor dynamic behavior and control Large PWRs typically use U-tube steam generators or horizontal steam generators, which are commonly found in VVER reactors (as shown in **Error! Reference source not found.**). In small modular reactors, the reduced reactor power creates an opportunity to utilize HCSGs.

Since the early days of the nuclear era, it has been appealing for nuclear engineers to incorporate steam generators and pressurizers within a Reactor Pressure Vessel (RPV) to eliminate external piping and the associated accidents, like Loss of Coolant Accidents (LOCA). Nowadays, some Small Modular Reactor (SMR) designs, such as NuScale, IRIS, and CAREM-25, have successfully implemented this concept. The most effective method for transferring heat from the primary to the

secondary system in these designs is through helical coil steam generators (HCSGs).

There are several advantages to using HCSGs compared to the current steam generators in commercial Pressurized Water Reactors (PWRs), including a compact design, higher heat transfer efficiency, and the ability to produce superheated steam.In order to develop a control system and conduct transient analysis, a robust dynamic model is needed to evaluate of the system's response to various scenarios and design a well-tuned controller. However, the presence of three phases on the secondary side and the different properties of the fluid in each region make dynamic simulation of this equipment complex.

HCSGs can be dynamically modeled using two approaches. The first approach utilizes the finite volume method with fixed boundaries. This method requires a large number of fine nodes to accurately track the boundary of each phase and utilize its characteristics. The second approach propose moving boundary model and coarse nodes. This method tracks boundary of phases with its special formulation so the necessity for using fine nodes obviates.

Using a movable boundary model for steam generator is computationally more efficient for these types of systems. Kerlin, Secker and Gilbert developed an HTGR steam generator model based on nine nodes in the HTGR OTSG [1,2]. In these simplified models, the secondary side is comprised of three nodes, with one node for each region.

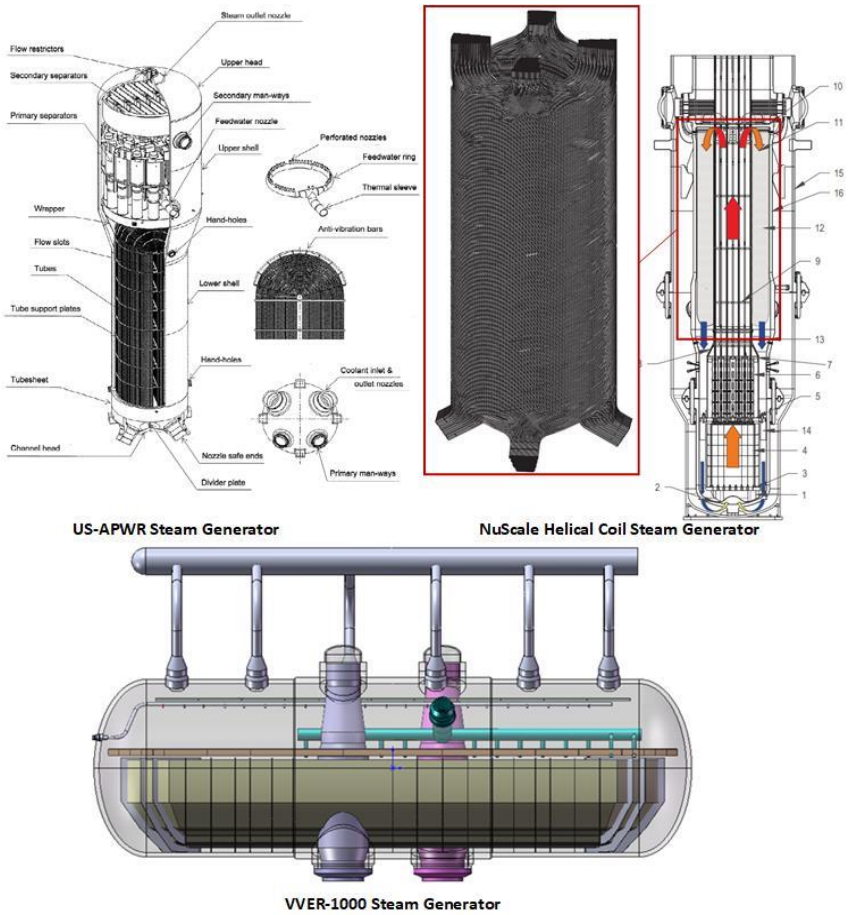

Fig. 1. Steam generator in different technologies of nuclear reactors [3-5].

Tzanos devised a movable boundary model for LMFBR [6,7]. In this work, a computer code named STEGA was written which was able to simulate LMFBR OTSG behavior. This model utilized different heat transfer models for nucleate boiling and film boiling regions. The set of equations was solved using a semi-analytic method for the steady-state condition. The Gear method implemented in the LSODE package for stiff differential equations was used for the integration of differential equations for the transient solution. Additionally, the proposed approach was benchmarked in a transient condition with the numerical experiment ETEC shutdown experiment that was carried out with the PSM-W numerical code [8].

Jensen and Tummescheit developed a 7th order model for the system and controller design of a multi-phase heat exchanger. This model utilized the slip ratio to calculate the mean average void fraction in the two-phase section. Additionally, Leibnitz's rule was applied for to convert the governing PDE equations to set of ODEs [9].

The main emphasis of our prior investigations was to develop a model using RELAP5 for the HCSG and other components of the NuScale reactor. The model was throughly validated against the reactor's design data and then utilized to simulate its response to different accident scenarios and transients [10,11]. In our earlier work, we formulated the basis for the HCSG model, which serves as the foundation of this study [12,13]. In the current work, the model has been enhanced, and the code's performance is evaluated under more intricate scenarios.

Due to the advantages of helical coil steam generators, this equipment has become a popular choice for usage in small modular reactors. The main objective of this work is to present an updated dynamic model with fast computation time for helical coil steam generators. This model would be applicable for designing this equipmentand could also be used for inspecting controller design. Due to the availability of data, NuScale has been chosen as the test case.

The developed model consists of a set of ordinary differential equations and takes advantage of both the moving boundary model and fine mesh approaches through by detecting boundaries of the phases and allowing each region to be divided into several computational nodes. To verify the code, results have been compared to the RELAP5 model of the HCSG.

2. Research theories

The steam generator is divided into three regions as shown in Fig. 2. Each region can be further divided into several nodes, with the lengths of the nodes in the primary system and tube metals varying based on their corresponding secondary nodes. The mathematical formulation for the secondary side is based on mass and energy balance equations, while only energy balance equations are needed for the tube metal section and primary side. The following assumptions have been made:

- Uniform secondary pressure,
- One-dimensional flow
- Negligible axial heat conductivity,
- No phase-change in the primary side,

- One equivalent helically-coiled tube in the SG.

Fig. 2 shows the schematic diagram of the implemented model for HCSG. The subcooled boundary extends from the secondary feedwater inlet to the point that fluid reaches the saturated enthalpy ($h \leq h_f$) while two-phase boundaries placed between the steam quality of ($0 < x < 1$) and superheat section $(h > h_g)$, Each region consists of numbers of nodes with the same lengths.

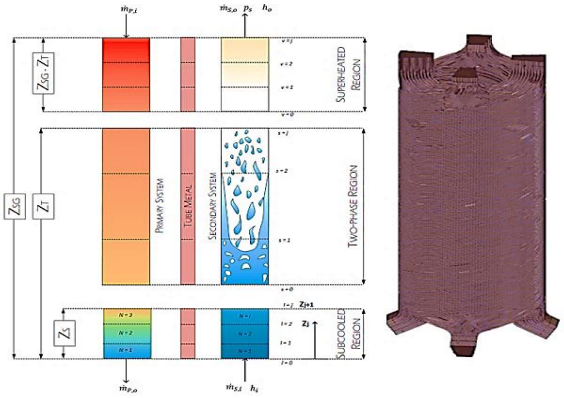

Fig. 2. HCSG model schematic.

The energy balance equation for the primary circut can be formulated as follows:

$$\rho C_p A_{pr}\left[(Z_{j+1}-Z_j)\frac{d\bar{T}_i}{dt}+(\bar{T}_i-\bar{T}_{i+1})\frac{dZ_{j+1}}{dt}\right] = n\pi D_o\alpha_o L_i(\bar{T}_{wi}-\bar{T}_{pi})+\dot{m}_p C_p(\bar{T}_{i+1}-\bar{T}_i) \quad (1)$$

By using this formula, a system of equations can be obtained for the primary system temperatures in each node. The upwind approximation is used for discretization of this equation. Table 1 shows the system of equations for primary system.

Table 1. System of equations for primary system.

Vol	Equation
1	$\dot{T}_{p1}=(f_{p1}-a_{p1,2}\dot{Z}_S)/a_{p1,1}$
2	$\dot{T}_{p2}=(f_{p2}-a_{p2,2}\dot{Z}_S)/a_{p2,1}$
3	$\dot{T}_{p3}=(f_{p3}-a_{p3,2}\dot{Z}_S)/a_{p3,1}$
4	$\dot{T}_{p4}=(f_{p4}-a_{p4,2}\dot{Z}_S-a_{p4,3}\dot{Z}_T)/a_{p4,1}$
5	$\dot{T}_{p5}=(f_{p5}-a_{p5,2}\dot{Z}_S-a_{p5,3}\dot{Z}_T)/a_{p5,1}$
6	$\dot{T}_{p6}=(f_{p6}-a_{p6,2}\dot{Z}_T)/a_{p6,1}$
7	$\dot{T}_{p7}=(f_{p7}-a_{p7,2}\dot{Z}_T)/a_{p7,1}$
8	$\dot{T}_{p8}=(f_{p8}-a_{p8,2}\dot{Z}_T)/a_{p8,1}$
9	$\dot{T}_{p9}=(f_{p9})/a_{p9,1}$

Metal heat transport is modeled using energy balance equations. These equations are written for each node. The characteristics of the tube metal are represented through:

$$C_w\rho_w A_w\left[(Z_{j+1}-Z_j)\frac{d\bar{T}_{w(i)}}{dt}+\frac{(\bar{T}_{w(i)}-\bar{T}_{w(i+1)})}{2}\frac{dZ_{j+1}}{dt}+\frac{(\bar{T}_{w(i-1)}-\bar{T}_{w(i)})}{2}\frac{dZ_j}{dt}\right] = n\pi\alpha_i D_i(Z_{j+1}-Z_j)(\bar{T}_{s(i)}-\bar{T}_{w(i)})+n\pi\alpha_o D_o(Z_{j+1}-Z_j)(\bar{T}_{p(i)}-\bar{T}_{w(i)}) \quad (2)$$

Writing this equation for nodes lead to system of equations represented in Table 2.

Table 2. System of equations for metal temperature.

Vol	Equation
1	$\dot{T}_{w1}=(1/a_{w1,1})*(f_{w1}-a_{w1,2}\dot{Z}_S)$
2	$\dot{T}_{w2}=(1/a_{w2,1})*(f_{w2}-a_{w2,2}\dot{Z}_S)$
3	$\dot{T}_{w3}=(1/a_{w3,1})*(f_{w3}-a_{w3,2}\dot{Z}_S)$
4	$\dot{T}_{w4}=(1/a_{w4,1})*(f_{w4}-a_{w4,2}\dot{Z}_S-a_{w4,3}\dot{Z}_T)$
5	$\dot{T}_{w5}=(1/a_{w5,1})*(f_{w5}-a_{w5,2}\dot{Z}_S-a_{w5,3}\dot{Z}_T)$
6	$\dot{T}_{w6}=(1/a_{w6,1})*(f_{w6}-a_{w6,2}\dot{Z}_S-a_{w6,3}\dot{Z}_T)$
7	$\dot{T}_{w7}=(1/a_{w7,1})*(f_{w7}-a_{w7,2}\dot{Z}_T)$
8	$\dot{T}_{w8}=(1/a_{w8,1})*(f_{w8}-a_{w8,2}\dot{Z}_T)$
9	$\dot{T}_{w9}=(1/a_{w9,1})*(f_{w9}-a_{w9,2}\dot{Z}_T)$

Mass and energy balance equations should be solved to simulate the secondary system performance. The mass balance for secondary can be expressed as:

$$A_s\left[(Z_{j+1}-Z_j)\frac{d\bar{\rho}_i}{dt}+(\bar{\rho}_{i-1}-\bar{\rho}_i)\frac{dZ_j}{dt}\right]=\dot{m}_{Z_j}-\dot{m}_{Z_{j+1}} \quad (3)$$

The number of unknowns will be equal to the number of equations if density is related to pressure and temperature in both the subcooled and superheated regions, and with void fraction in the two-phase section.

Table 3. Mass balance equations for the secondary system.

Vol	Equation
1	$a_{1,1}\dot{P}_s + a_{1,2}\dot{h}_1 = f_{m1}$
2	$a_{2,1}\dot{P}_s + a_{2,2}\dot{h}_2 + a_{2,3}\dot{Z}_s = f_{m2}$
3	$a_{3,1}\dot{P}_s + a_{3,2}\dot{Z}_s = f_{m3}$
4	$a_{4,1}\dot{P}_s + a_{4,2}\dot{\alpha}_1 + a_{4,3}\dot{Z}_S = f_{m4}$
5	$a_{5,1}\dot{P}_s + a_{5,4}\dot{\alpha}_2 + a_{5,3}\dot{Z}_S + a_{5,4}\dot{Z}_T = f_{m5}$
6	$a_{6,1}\dot{P}_s + a_{6,2}\dot{Z}_S + a_{6,3}\dot{Z}_T = f_{m6}$
7	$a_{7,1}\dot{P}_s + a_{7,2}\dot{h}_7 + a_{7,3}\dot{Z}_T = f_{m7}$
8	$a_{8,1}\dot{P}_s + a_{8,2}\dot{h}_8 + a_{8,3}\dot{Z}_T = f_{m8}$
9	$a_{9,1}\dot{P}_s + a_{9,2}\dot{h}_9 + a_{9,3}\dot{Z}_T = f_{m9}$

Furthermore, secondary system energy balance is:

In the two-phase section, the heat transfer coefficient value significantly decreases in the post-dry-out regime compared to other areas within the same section. To address this issue, the Levitan and Borevskiy correlation has been utilized to identify nodes positioned in the post-dry-out region.

Table 4. Energy balance equations for secondary system.

Vol	Equation
1	$b_{1,1}\dot{P}_s + b_{1,2}\dot{h}_1 = f_{e1}$
2	$b_{2,1}\dot{P}_s + b_{2,2}\dot{h}_2 + b_{2,3}\dot{Z}_s = f_{e2}$
3	$b_{3,1}\dot{P}_s + b_{3,2}\dot{Z}_s = f_{e3}$
4	$b_{4,1}\dot{P}_s + b_{4,2}\dot{\alpha}_1 + b_{4,3}\dot{Z}_S = f_{e4}$
5	$b_{5,1}\dot{P}_s + b_{5,4}\dot{\alpha}_2 + b_{5,3}\dot{Z}_S + b_{5,4}\dot{Z}_T = f_{e5}$
6	$b_{6,1}\dot{P}_s + b_{6,2}\dot{Z}_S + b_{6,3}\dot{Z}_T = f_{e6}$
7	$b_{7,1}\dot{P}_s + b_{7,2}\dot{h}_7 + b_{7,3}\dot{Z}_T = f_{e7}$
8	$b_{8,1}\dot{P}_s + b_{8,2}\dot{h}_8 + b_{8,3}\dot{Z}_T = f_{e8}$
9	$b_{9,1}\dot{P}_s + b_{9,2}\dot{h}_9 + b_{9,3}\dot{Z}_T = f_{e9}$

$$\begin{cases} \frac{d\bar{\rho}_i}{dt} = \frac{\partial\rho_i}{\partial P_s}\Big|_h \frac{dP_s}{dt} + \frac{\partial\rho_i}{\partial h_i}\Big|_{P_s}\frac{dh_i}{dt} \text{ for subcooled and superheat section} \\ \frac{d\bar{\rho}_i}{dt} = \left(\frac{\partial\rho_f}{\partial P_s} + \frac{\partial\rho_f}{\partial h_f}\frac{\partial h_f}{\partial P_s}\right)\frac{dP_s}{dt} \text{for saturated node} \\ \frac{d\bar{\rho}_i}{dt} = \rho_{fg}\frac{d\alpha_i}{dt} + \left(\alpha_i\frac{d\rho_{fg}}{dP_s} + \frac{d\rho_f}{dP_s}\right)\frac{dP_s}{dt} \text{for two} - \text{phase section} \end{cases} \quad (4)$$

$$A_s\left[(Z_{j+1}-Z_j)h_i\frac{d\bar{\rho}_i}{dt} + (Z_{j+1}-Z_j)\rho_i\frac{dh_i}{dt} - (Z_{j+1}-Z_j)\frac{dP_i}{dt} + (\rho_{i-1}h_{i-1}-\rho_i h_i)\frac{dZ_j}{dt}\right] = \dot{m}_{i-1}h_{i-1} - \dot{m}_i h_i + n\pi D_i\alpha_i(Z_{j+1}-Z_j)(\bar{T}_{w(i)} - \bar{T}_{s(i)}) \quad (5)$$

$$x_{ad} = 2.7\left(\frac{\rho_f\sigma}{G^2 d}\right)^{1/4}\left(\frac{\rho_g}{\rho_f}\right)^{1/3} \quad (6)$$

For nodes with steam quality of more than x_{ad} Chen and Chen's formula is used to calculate the heat transfer coefficient. Steam mass flow rate that flows toward the turbine is obtained from:

$$\dot{m}_{turbine} = K_c\sqrt{P_{SG} - P_{turbine}} \quad (7)$$

The detail of mathematical model and its derivation process is elaborated in with detail in [12].

2.1. HCSG RELAP5 model

The RELAP5 code is employed to evaluate performance of the developed model. This model uses the fixed node approach. For this reason, the helical part of the steam generator is divided into 30 nodes as shown in Fig. 3. The

shell part of the HCSG is modeled using an annulus component comprised of 32 nodes. Vertical bundle with crossflow is the closest heat transfer model which can be used for this component. For this reason, this model is enabled for primary flow.

The boundary condition of the HCSG is modeled using a combination of time-dependent volumes, time-dependent junctions and single junction components. Tube side of steam generators which is comprising 1380 tubes is modeled using series of pipes with equivalent inclination angle, length and flow area. A summary of the steam generator is brought in Table 5.

Table 5. Specification of the NuScale reactor steam generator [14].

Parameter	value	Unit
Number of steam generators per NPM	2	
Number of helical tubes per steam generator	690	
Outer diameter of tubes	1.59	cm
Tube wall thickness	0.127	cm
Average length of tubes	24.2	m
Feedwater temperature	421.87	K
Main steam temperature range at nominal power	574.8-580.4	K
Outlet pressure	3.45	MPa

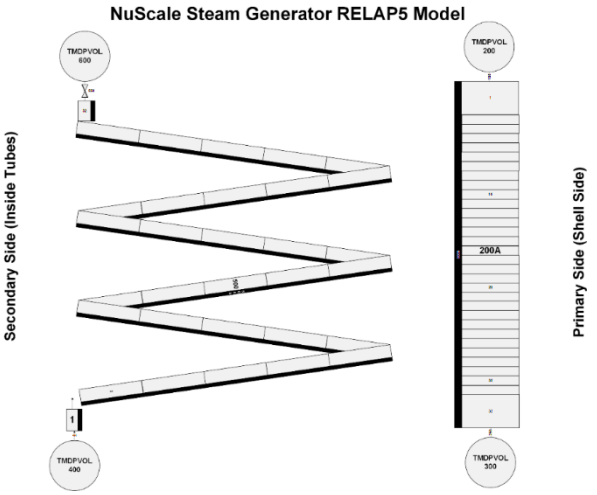

Fig. 3. RELAP5 model of HCSG.

3. Results and discussion

The steady-state results calculated from RELAP5 and the developed model are demonstrated in Table 6. The results show a good agreement between the models and the design data of the reactor. Furthermore, the temperature profile in steady-state conditions calculated by the mathematical model is illustrated in Fig. 4. It can be seen that this model calculates the temperature profile in each phase with more accuracy compared to previous works [15].

Table 6. Steady-State performance of the models.

	Design data	**RELAP5**	**Current model**
Core outlet Temperature (K)	585.9	585.9	585.9
Core inlet Temperature (K)	533.7	535.16	533.9
Feedwater inlet Temperature (K)	421.9	421.9	421.87
Steam outlet temperature (K)	575 - 580	579.83	579.73
Steam pressure (MPa)	3.45	3.45	3.45

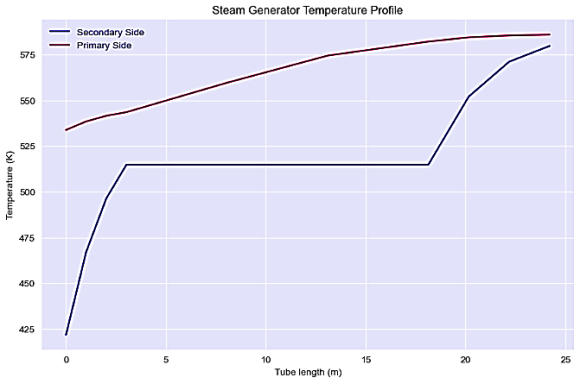

Fig. 4. HCSG temperature profile for primary and secondary side based on developed model.

In this study, two scenarios are considered to evaluate model performance during transient conditions. The details of these scenarios are provided in the following sections.

3.1. Ramp changes of the feedwater flow rate

In this scenario, as depicted in Fig. 5 (a), it is assumed that a gradual decrease in the feedwater flow rate begins at 100 seconds. Over a span of 300 seconds, the feedwater is reduced by 5%. Subsequently.The feedwater value remains constant for 10 minutes, after which it gradually increases over a duration of 1 minute to its nominal value. The results from the two codes are compared in Fig. 5, showing a similar trend of changes for both codes.

The pressure of the secondary system is directly related to the feedwater flow rate, this means that as the feedwater flow increases, the pressure in the steam generator also increases. This relationship is demonstrated in Fig. 5 (c), which displays the pressure variation during the transient and highlights its proportional correlation with the feedwater flow. It is worth noting that both codes calculated the same value for the pressure decrease in the given scenario.

Accurately calculating the primary side outlet temperature is crucial because its fluctuations can impact the core inlet temperature. Fig. 5 (b) depicts the response of the primary side outlet temperature to the transient feedwater. The results indicate that both RELAP5 and the developed code accurately calculate the same temperature increase during the transient for the core inlet temperature. Fig. 5 (d) demonstrates the impact of a 5% ramp decrease and subsequent increase in feedwater flow rate on the steam temperature. It reveals that the steam temperature rises accordingly, aligning with the expected behavior. While both methods employed exhibit a consistent trend in steam temperature, there are slight differences of approximately 1 degree in the final values. This difference can be attributed to the significantly lower specific heat capacity of the superheat section and its sensitivity in the case study SG compared to the primary and other SG sections. As a result, even minor disparities between the heat transfer models and the length of the superheat section can lead to temperature variations between RELAP5 and the mathematical model.

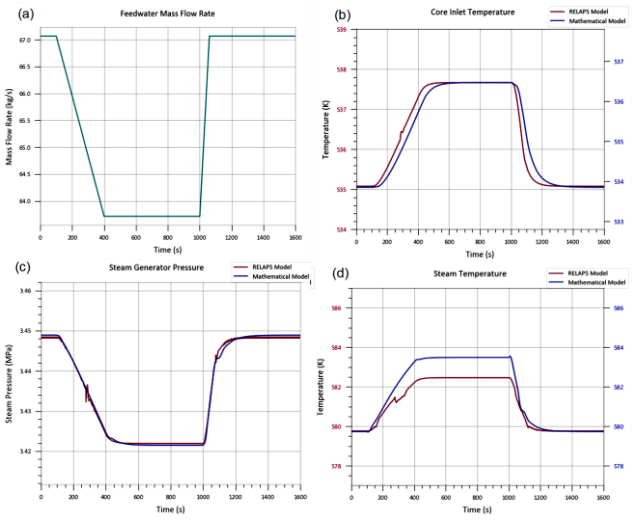

Fig. 5. System response to the 5% ramps in feedwater flow rate.

3.2. Impact of Mass Flow Rate and SG Inlet Temperature Variation

The primary system's temperatures and flow are interconnected in the NuScale reactor's primary loop, which operates through natural circulation. This means that any power transient in the core leads to fluctuations in both the primary flow rates and temperatures.
In this section, a scenario is considered to evaluate the capability of the developed model in simulating situations where multiple input parameters change. Using the RELAP5 reactor model that was developed in previous research [10], ramp reactivities were introduced into the reactor core, and the inlet parameters for the HCSG, which serve as inputs for the developed model, were calculated. These inputs are presented in Fig. 6 (a, b, c). Thethe next step involved analyzing the response of the developed model to assess its calculation performance.

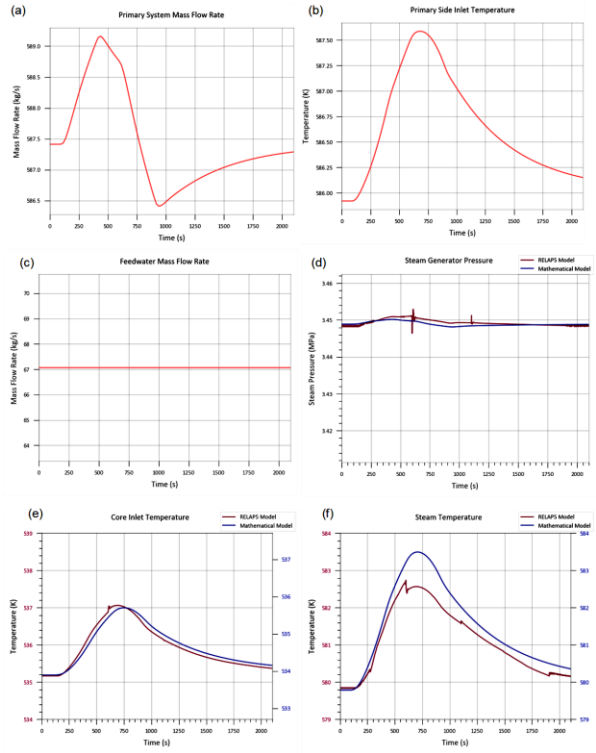

Fig. 6. System response to transients in primary parameters.

In this particular scenario, both the mass flow rate and inlet temperature of the primary circuit undergo changes over time. The results indicate that an increase in the inlet temperature of the SG leads to a corresponding rise in the steam outlet temperature, as illustrated in Fig. 6 (f). Additionally, the variation in the primary mass flow rate has an impact on the secondary pressure, as shown in Fig. 6 (d).

In this scenario, an increase in the primary inlet temperature causes an elevation in the steam temperature. However, the secondary side of the system is unable to effectively remove all the generated power from the primary. Consequently, the primary exit temperature experiences an increase, as depicted in Fig. 6 (e).

The results demonstrate that both codes produce similar trends. However, there are instances where the RELAP5 results exhibit discontinuities, such as at 600 seconds in Fig. 6 (f). To assign accurate heat transfer coefficients to each volume, codes with fixed nodes are required to determine the flow regime at each time step. Consequently, during points of flow regime changes in certain nodes, it is noticeable that some discontinuities emerge in the results when using the moving boundary model. This model, however, is capable of calculating the results with greater precision because there is no physical phenomenon that corresponds to these discontinuities.

4. Conclusions

In this research, the performance of the multi-node moveable boundary model is evaluated and compared with the RELAP5 code. The secondary side of SG is divided into three regions and linked with primary and tube metal

equations. Each region has its own formulation and heat transfer coefficients. Calculated results show a good agreement between the design data of the reactor and simulations. Additionally, a RELAP5 model of SG is developed. The model's response to several transients in the model's inputs is calculated and compared with the RELAP5 code. It is observed that the trend of transient responses was similar in all cases. The change in final values for pressure and primary outlet temperature was in good agreement between the developed model and RELAP5. Due to the different nature of equations and solving methods of the two codes, there was a slight difference between the results for steam temperature. However, the overall behaviors were identical.

Conflict of interest

The authors declare no potential conflict of interest regarding the publication of this work.

References

[1] Secker, P. and J. Gilbert, Status of CHAP: composite HTGR analysis program. 1975, Los Alamos Scientific Lab.

[2] Kerlin, T., HTGR steam generator modeling. 1976, Oak Ridge National Lab.

[3] Industries, M.H., DESIGN CONTROL DOCUMENT FOR THE US-APWR. 2013: Nuclear Regulatory Commission.

[4] NuScale power LLC, NuScale Status in the Regulatory Process. 2017: http://www.nuscalepower.com/our-technology/nrc-interaction/.

[5] Atomenergoproekt, Final safety analysis report of BNPP's VVER-1000 reactor. 2015: Moscow.

[6] Tzanos, C.P., A semianalytic method for the solution of the steady-state steam generator equations. Nuclear Technology, 1988. **80**(3): p. 380-391.

[7] Wu, Y., et al., A movable boundary model for helical coiled once-through steam generator using preconditioned JFNK method. International Journal of Advanced Nuclear Reactor Design and Technology, 2022. **4**(1): p. 1-8.

[8] Berry, G., Model of a once-through steam generator with moving boundaries and a variable number of nodes. 1983, Argonne National Lab., IL (USA).

[9] Jensen, J.M. and H. Tummescheit. Moving boundary models for dynamic simulations of two-phase flows. In Proc. of the 2nd int. Modelica conference. 2002. Oberpfaffhenhofen Germary.

[10] Fakhraei, A., et al., Safety analysis of an advanced passively-cooled small modular reactor during station blackout scenarios and normal operation with RELAP5/SCDAP. Annals of Nuclear Energy, 2020. **143**: p. 107470.

[11] Fakhraei, A., et al., Coolant flow rate instability during extended station blackout accident in NuScale SMR: Two approaches for improving flow stability. Progress in Nuclear Energy, 2021. **131**: p. 103602.

[12] Fakhraei, A., et al., DYSN: Dynamics simulator for the NuScale SMR-A mathematical framework for transient analysis. Progress in Nuclear Energy, 2024. **170**: p. 105128.

[13] Fakhraei, A., F. Faghihi, and M. Mohammadi, A Multi-Node Moving Boundary Model for Transient Dynamics of Nuscale Smr Steam Generator and Designing a Controller Using Fuzzy Logic and Pid. Available at SSRN 4421440.

[14] NuScale Power LLC, NuScale Standard Plant Design Certification Application. 2020: U.S. Nuclear Regulatory Commission (NRC).

[15] Arda, S.E. and K.E. Holbert, Nonlinear dynamic modeling and simulation of a passively cooled small modular reactor. Progress in Nuclear Energy, 2016. **91**: p. 116-131.

How to cite this article
A. Fakhraei, F. Faghihi, *Development of Transient Dynamics Code for a Helically-Coiled Steam Generator Analysis Using Multi-Node Moving Boundary Model*, Journal of Nuclear Research and Applications (JONRA), Volume 5 Number 1 Winter (2025) 21-30, **URL:** https://jonra.nstri.ir/article_1701.html, **DOI:** https://doi.org/10.24200/jonra.2024.1626.1134.